

Metal-Free Tetrathienoacene Sensitzers for High-Performance Dye-Sensitized Solar Cells

Nanjia Zhou,^{†,#} Kumaresan Prabakaran,^{‡,∇,#} Byunghong Lee,^{†,#} Sheng Hsiung Chang,[§]
Boris Harutyunyan,[†] Peijun Guo,[†] Melanie R. Butler,^{||} Amod Timalsina,^{||} Michael J. Bedzyk,^{*,†}
Mark A. Ratner,^{*,||} Sureshraju Vegiraju,[‡] Shuehlin Yau,[‡] Chun-Guey Wu,^{‡,§} Robert P. H. Chang,^{*,†}
Antonio Facchetti,^{*,||,⊥} Ming-Chou Chen,^{*,‡} and Tobin J. Marks^{*,||}

[†]Department of Materials Science and Engineering and the Materials Research Center, the Argonne-Northwestern Solar Energy Research Center, Northwestern University, 2145 Sheridan Road, Evanston, Illinois 60208, United States

[‡]Department of Chemistry, National Central University, Chung-Li, Taiwan 32054, ROC

[§]Research Center for New Generation Photovoltaics, National Central University, Chung-Li, Taiwan 32054, ROC

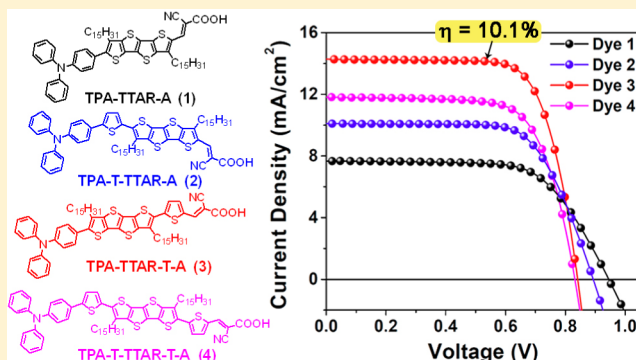
^{||}Department of Chemistry and the Materials Research Center, the Argonne-Northwestern Solar Energy Research Center, Northwestern University, 2145 Sheridan Road, Evanston, Illinois 60208, United States

[⊥]Polyera Corporation, 8045 Lamon Avenue, Skokie, Illinois 60077, United States

[∇]Department of Chemistry, PSG College of Arts and Science, Coimbatore, India-641014

Supporting Information

ABSTRACT: A new series of metal-free organic chromophores (TPA-TTAR-A (**1**), TPA-T-TTAR-A (**2**), TPA-TTAR-T-A (**3**), and TPA-T-TTAR-T-A (**4**)) are synthesized for application in dye-sensitized solar cells (DSSC) based on a donor- π -bridge-acceptor (D- π -A) design. Here a simple triphenylamine (TPA) moiety serves as the electron donor, a cyanoacrylic acid as the electron acceptor and anchoring group, and a novel tetrathienoacene (TTA) as the π -bridge unit. Because of the extensively conjugated TTA π -bridge, these dyes exhibit high extinction coefficients ($4.5\text{--}5.2 \times 10^4 \text{ M}^{-1} \text{ cm}^{-1}$). By strategically inserting a thiophene spacer on the donor or acceptor side of the molecules, the electronic structures of these TTA-based dyes can be readily tuned. Furthermore, addition of a thiophene spacer has a significant influence on the dye orientation and self-assembly modality on TiO₂ surfaces. The insertion of a thiophene between the π -bridge and the cyanoacrylic acid anchoring group in TPA-TTAR-T-A (dye **3**) promotes more vertical dye orientation and denser packing on TiO₂ (molecular footprint = 79 Å²), thus enabling optimal dye loading. Using dye **3**, a DSSC power conversion efficiency (PCE) of 10.1% with $V_{oc} = 0.833 \text{ V}$, $J_{sc} = 16.5 \text{ mA/cm}^2$, and FF = 70.0% is achieved, among the highest reported to date for metal-free organic DSSC sensitizers using an I⁻/I₃⁻ redox shuttle. Photophysical measurements on dye-grafted TiO₂ films reveal that the additional thiophene unit in dye **3** enhances the electron injection efficiency, in agreement with the high quantum efficiency.



INTRODUCTION

Since the first successful demonstration of dye-sensitized solar cells (DSSCs) based on a polypyridyl ruthenium(II) dye,¹ the past decade has witnessed a steady increase of power conversion efficiencies (PCEs) for metal complex-sensitized DSSCs.² While each device component optimization has impacted the progress of this technology, the understanding-based development of more effective sensitizers is undoubtedly one of the most promising components to investigate for further advances in PCE.^{3–5} Among these sensitizers, the most prominent examples are the zinc porphyrin sensitizers SM371 and SM315 (Scheme 1A), which provide PCEs of 12.5–13.0% when employing a Co(II/III) redox shuttle as the electrolyte

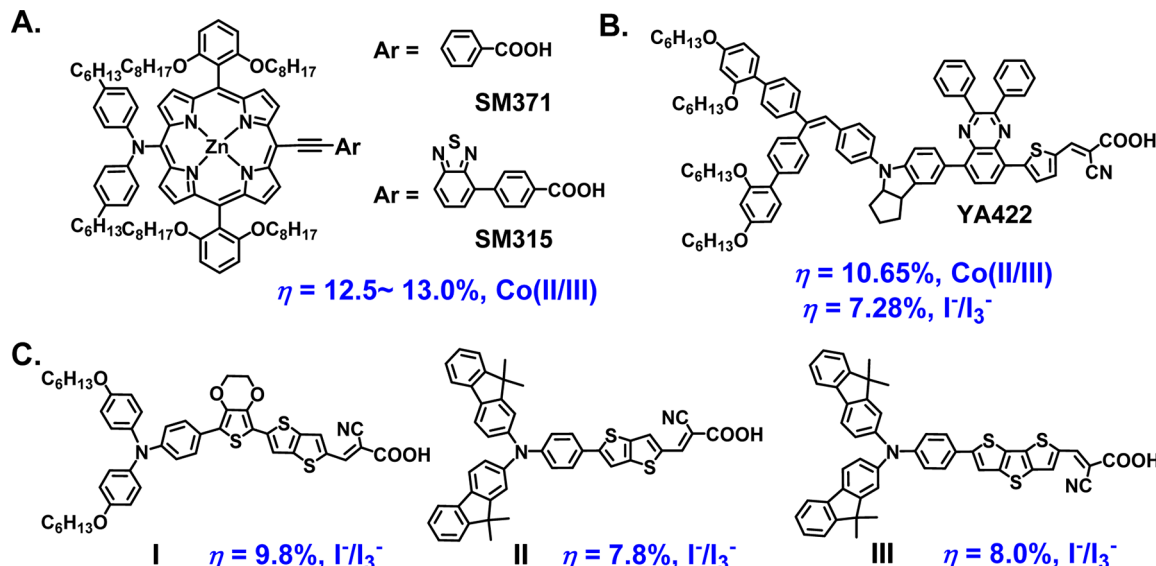
system.^{2,6,7} With the goal of broadening our understanding of DSSC function and performance limitations, metal-free organic photosensitizers have attracted great recent attention owing to their (a) chemical versatility and facile synthetic approaches to diverse molecular structures; (b) energetic and structural tunability to realize broad and high levels of solar spectral absorption (sizable molar extinction coefficients) within the visible region, and in some cases, the near-IR region as well; (c) potential cost reductions vs DSSCs employing noble metal containing dyes.^{8–11} Nevertheless, despite these attractions, to

Received: December 30, 2014

Published: March 13, 2015



Scheme 1. Examples of (A) Zinc Porphyrin-Based DSSC Dyes, (B) the Highest PCE Metal-Free Organic Dye Reported to Date, and (C) Metal-Free Fused Thiophene-Based D- π -A Dyes^a



^aPower conversion efficiencies and redox shuttle employed are given in blue.

date the performance of DSSCs based on metal-free organic dyes has lagged behind those using traditional metal-organic dyes, largely as a result of their high recombination losses and lower open circuit voltages (V_{oc}).^{12–14} However, note that a few recent reports have shown PCEs = 10.0–10.65% employing single metal-free organic dyes (e.g., YA442, Scheme 1B) in combination with a Co(II/III) redox shuttle, demonstrating the potential of this approach.^{15–20}

The design of molecular DSSC dyes requires careful consideration of multiple optoelectronic properties, such as band alignment and optical absorption coefficient, as well as solid-state properties such as dye aggregation, morphology, and mode of assembly on the TiO₂ photoanode.^{21–23} A promising strategy for organic sensitizer design employs a donor- π -bridge-acceptor (D- π -A) framework that can satisfy these requirements.^{24–28} Among them, most organic dyes typically feature a hydrophobic electron-donating triphenylamine (TPA) moiety connected via a π -conjugated bridge unit to an hydrophilic electron-accepting cyanoacrylic acid group which acts as the anchoring site on the TiO₂ photoanode (Scheme 1 and Figure 1).^{27,29–31} For this class of dyes, the traditional focus has been to design π -conjugated spacer units which facilitate charge transfer from the ground to excited state and increase light absorption. Representative bridging units often employ well-known π -conjugated thiophene systems, such as oligothiophenes, thienylene-vinylenes, in addition to fused thiophenes, including thienothiophenes (TT) and dithienothiophene (DTT).^{32–35} These systems afford excellent efficiencies, up to 9.8% (I; Scheme 1).³⁵ Note that there are several potential advantages to further extending the bridge such as a smaller band gap for extended light absorption and a better match with the energetics of the I⁻/I₃⁻ redox shuttle, thereby enhancing DSSC charge transfer characteristics. For example, organic dyes based on the simplest fused thiophene, TT, enable PCEs up to 7.8% (II; Scheme 1),³² while with a more conjugated DTT, the maximum PCE is increased to 8.0% (III; Scheme 1).³⁴ Toward creating even more conjugated structures, an attractive organic dye design would be to introduce a highly planar

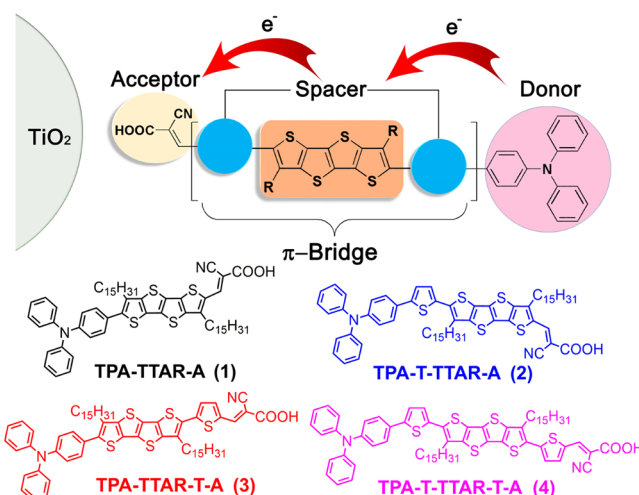
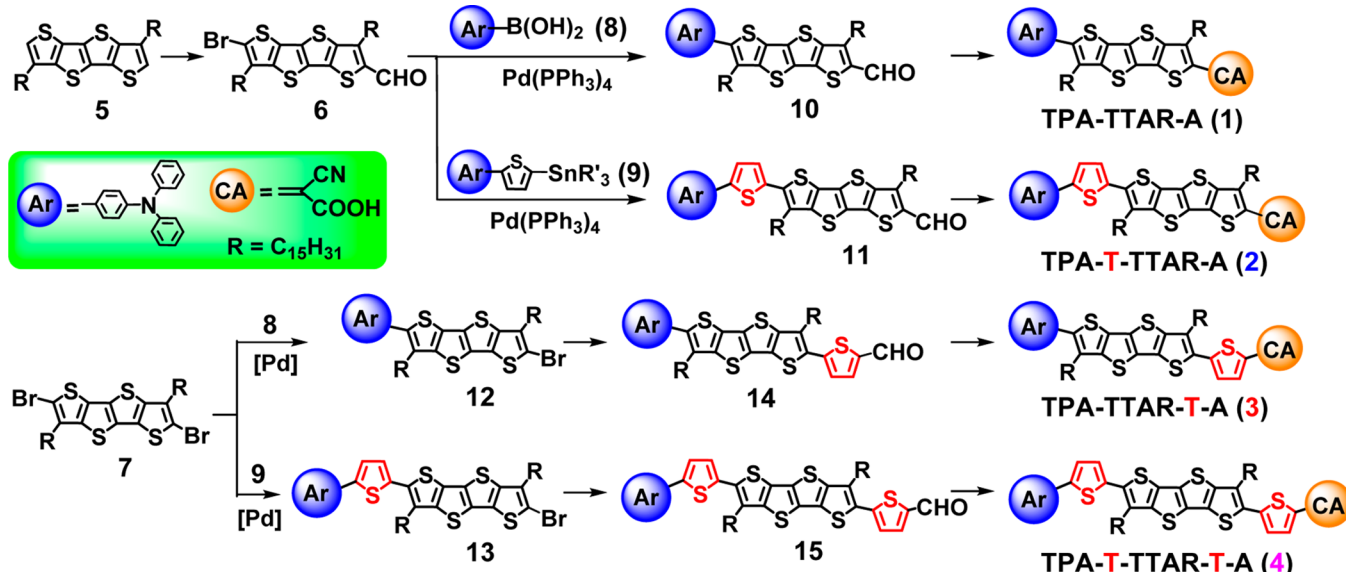


Figure 1. Schematic representation of the donor- π -bridge-acceptor molecular dye design concept and the chemical structures of TTA dyes 1–4.

tetrathienoacene (TTA) core as the π -bridge unit.³⁶ We previously disclosed that this unit features strong intramolecular S-S interactions enabling long-range order in the solid state and excellent charge transport in organic thin film transistors (OFETs) with hole/electron mobilities as high as 0.42 and 0.30 cm² V⁻¹ s⁻¹, respectively.^{37,38}

With the premise that additional core extension should enhance DSSC performance even further, here we introduce a new TTA-based sensitizer series. To maintain adequate dye processability, we have introduced a long alkyl substituent (R = *n*-C₁₅H₃₁) on the TTA core in all sensitizers, which also suppresses dye aggregation and charge recombination on the TiO₂ surface. In addition, we systematically investigate the effects of thiophene introduction between the bridge and the donor and/or acceptor moieties. Starting from the simplest TTAR structure, TPA-TTAR-A (dye 1), a thiophene spacer is either inserted on the donor side between TTAR and TPA to

Scheme 2. Synthetic Routes to Metal-Free DSSC Sensitizers 1–4



yield TPA-T-TTAR-A (dye 2), or on the acceptor side between TTAR and cyanoacrylic acid to yield TPA-TTAR-T-A (dye 3), and finally on both sides to yield TPA-T-TTAR-T-A (dye 4) (Figure 1). These π -extended systems should enhance panchromatic light-harvesting, as the result of the uplifted TTA highest occupied molecular orbital (HOMO) and lower lowest unoccupied molecular orbital (LUMO) compared to TT and DTT based molecules.^{37,39} In this work, a simple, baseline iodine-based electrolyte is employed to investigate the DSSC characteristics. It will be seen that the additional thiophene spacer provides a simple strategy to modify the optoelectronic, chemical and physical properties of these organic sensitizers, and thereby enhance DSSC PCEs.

RESULTS AND DISCUSSION

In the following section we discuss the design rationale and the synthesis of new metal-free DSSC dyes 1–4. Next, these systems are characterized at the molecular level using optical spectroscopy, molecular orbital computations, and cyclic voltammetry (CV). Subsequently, DSSC devices are fabricated using these dyes to evaluate performance metrics. To better understand the device response, electrochemical impedance (EIS) analysis is performed on the DSSCs, and dye molecular orientation and coverage are characterized by X-ray reflectivity (XRR) and optical spectroscopic measurements. Finally, femtosecond time-resolved photoluminescence (FTR-PL) measurements are performed to investigate in detail the photophysical processes operative in these organic dyes.

Synthetic Strategy. The synthetic approaches to dyes 1–4 are presented in Scheme 2. Dyes 1 and 2 are obtained by reacting bromoformyltetrathienoacene (6) with the corresponding amino-donor moieties 8 and 9 via Suzuki and Stille coupling protocols to give formylated tetrathienoacenes 10 and 11, respectively. The resulting TTAs are then reacted with cyanoacetic acid in a Knoevenagel condensation to yield dyes 1 and 2 in good yields. Dyes 3 and 4 were synthesized from dibromotetrathienoacene (7) in good yields via three steps. First, dibromotetrathienoacene (7) is monocoupled with the corresponding amino-donor moieties 8 and 9 to afford the monobrominated tetrathienoacenes, 12 and 13, respectively.

Second, the resulting TTAs are then linked with 5-(1,3-dioxolan-2-yl)thiophen-2-yltributylstannane via Stille coupling to yield the corresponding aldehydes 14 and 15. Finally, both aldehydes are then treated with cyanoacetic acid in the presence of piperidine to afford dyes 3 and 4. Note, the preparation of dyes 1 and 2 from the intermediate 7 was not successful. As shown in Scheme 2, 6 was prepared by monoformylation of TTA (5) via a Vilsmeier–Haack protocol, followed by bromination. Detailed synthetic procedures are described in the Supporting Information (SI).

Characterization of Dyes 1–4. The optical absorption spectra of the four new dyes in 1,2-dichlorobenzene (*o*-DCB) solution are shown in Figure 2, indicating the presence of two strong absorptions assignable to a charge-transfer (CT) band [\sim 498 nm (1), \sim 482 nm (2), \sim 490 nm (3), \sim 513 nm (4)] and a higher energy π – π^* transition [\sim 340 nm (1), \sim 389 nm (2), \sim 369 nm (3), \sim 402 nm (4)]. Importantly, the insertion of one or two thiophenes in dyes 2–4 noticeably red-shifts the absorption onset compared to dye 1 as a result of their extended conjugation lengths. All four dyes 1–4 exhibit large molar extinction coefficients at their absorption maxima, with values \sim 3–4× larger than those of typical Ru(II) polypyridyl complexes (N719; 1.40×10^4 M^{−1} cm^{−1}).⁴⁰ Therefore, these dyes are expected to efficiently harvest light and enable large photocurrents in a DSSC device.⁴¹

To estimate the energy level alignment of dyes 1–4 versus TiO₂ and the I[−]/I₃[−] redox mediator, CV measurements were performed in solution with addition of ferrocene as the internal standard (Figure 3a). All four dyes exhibit two distinct and reversible oxidations without any reductive features.²⁶ HOMO energies of the four dyes were estimated from the onset potentials (E_{ox}) of the first oxidation peaks; $E_{\text{HOMO-CV}} = -(4.8 + E_{\text{ox}})$,⁴² and found to be -5.29 , -5.16 , -5.22 , and -5.09 eV for dyes 1–4, respectively. Evidently, the addition of the thiophene spacer(s) into dye 1 upshifts the HOMO energies. This result, combined with the HOMO and LUMO energy gap contraction on going from 1 (2.18 eV) to 2/3 (2.08 eV) to 4 (2.04 eV) as indicated by the optical spectroscopy data (Figure S3), yields a dye independent LUMO energy of \sim 3.1 eV for all dyes.¹⁷

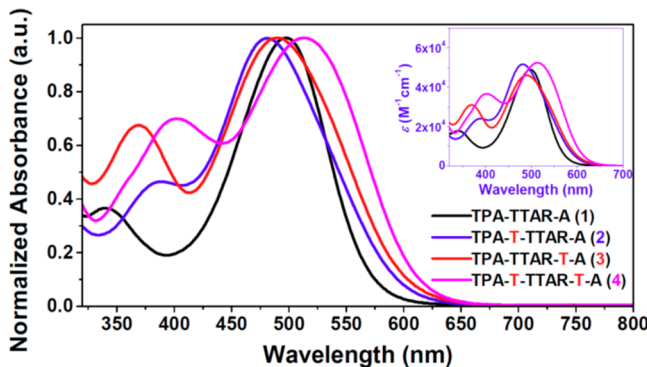


Figure 2. UV-vis absorption spectra of dyes **1–4** and their corresponding molar absorption coefficients measured in *o*-DCB in concentration of 10^{-5} M.

Electronic structure calculations were performed at the B3LYP/6-31G** level of density functional theory (DFT; Figures 3c and S1). Figure 3c shows a representation of the HOMO and LUMO topologies for dyes **1–4** (Table 1), indicating that the HOMOs are clearly more localized at the TPA donor moieties while the LUMOs are primarily localized on the cyanoacrylic acid unit.⁴³ Such a directional electronic distribution is ideal for electron injection into TiO_2 from anchoring sites and reduction of oxidized dyes by I^-/I_3^- .²⁹ Importantly, the DFT computed HOMO energies are in excellent agreement with the experimental HOMO energies estimated from CV measurements (Figure 2a). Regarding the DFT-calculated dye geometries, the insertion of a thiophene spacer in between the TPA and the TTA units (dyes **2** and **4**), noticeably reduces core planarity (Figure S1), possibly suggesting nonideal dye assembly and hampered charge injection characteristics (See more below).³⁰

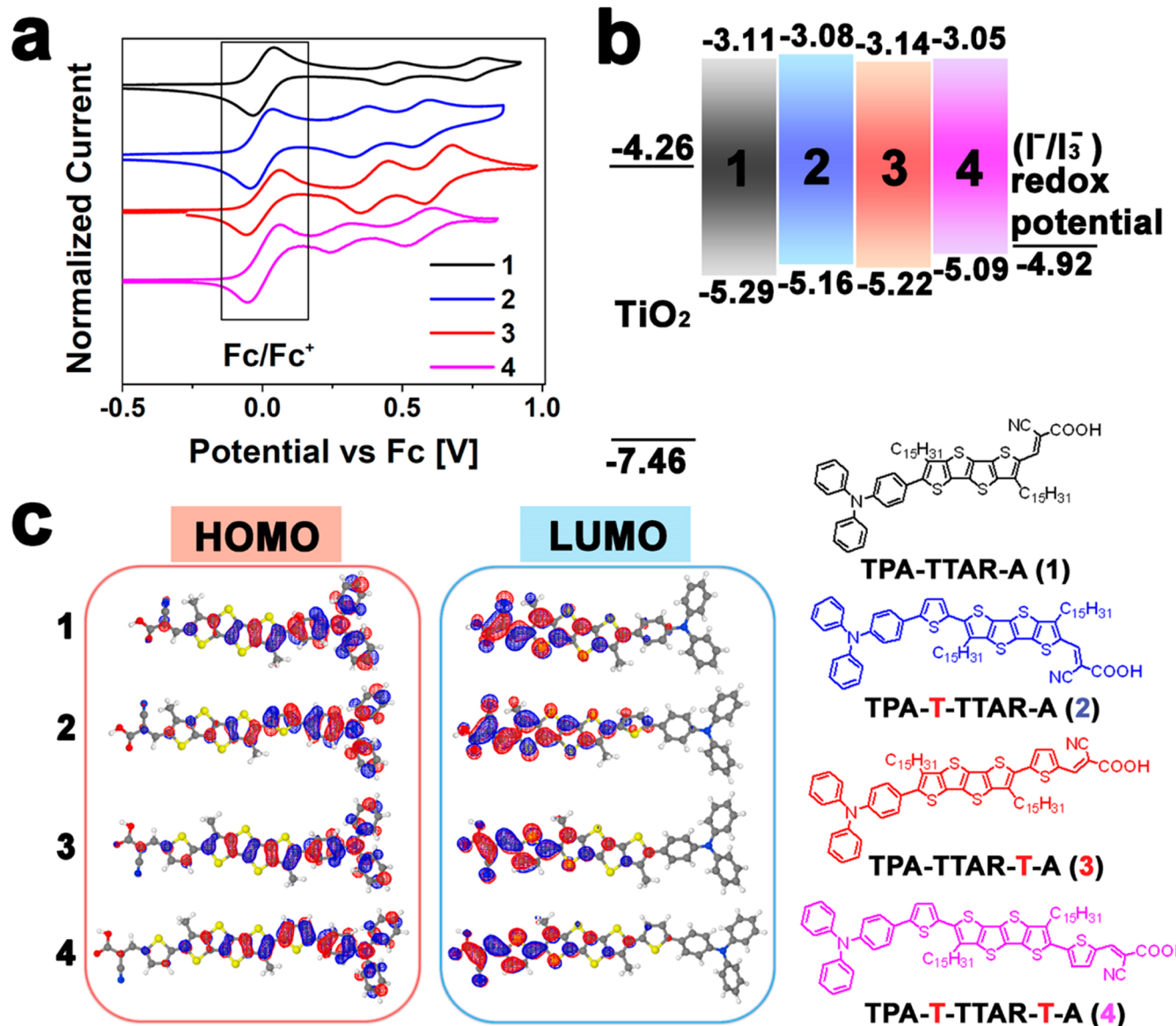


Figure 3. Electronic structure characterization of dyes **1–4**. (a) Solution cyclic voltammograms with the midpoint potential of the ferrocene/ferrocenium (Fc/Fc^+) internal standard referenced to 0.0 V. (b) MO energy diagram with respect to the conduction band of TiO_2 , where the HOMO levels are determined from the onset of first oxidation peak, and LUMO levels are derived from HOMO–LUMO energy gap from optical measurements on films. (c) Isodensity surface plots for the HOMO and the LUMO of dyes **1–4**.

Table 1. Summary of Optical and Electrochemical Properties of Dyes 1–4

dye	UV-vis λ_{max}^a (nm)	$E_{\text{HOMO-CV}}^b$ (eV)	$E_{\text{HOMO-DFT}}^c$ (eV)	E_{LUMO}^d (eV)	$E_{\text{LUMO-DFT}}^c$ (eV)	ΔE_g^e (eV)	ΔE_g^c (eV)	μ (Debye)
1	498	-5.29	-5.12	-3.11	-2.64	2.18	2.48	11.3
2	482	-5.16	-5.01	-3.08	-2.69	2.08	2.32	11.5
3	490	-5.22	-5.06	-3.14	-2.78	2.08	2.28	7.65
4	513	-5.09	-4.95	-3.05	-2.80	2.04	2.15	7.79

^aMeasured in *o*-DCB at a concentration of 10^{-5} M⁻¹. ^b $E_{\text{HOMO-CV}} = -(4.8 + E_{\text{ox}})$ where E_{ox} = Onset potential of the first oxidation peak when the Fc/Fc+ internal standard is referenced to 0.0 V. ^cBy DFT calculation. ^dEstimated from $E_{\text{HOMO}} + \Delta E_g$. ^e ΔE_g calculated from absorption onsets.

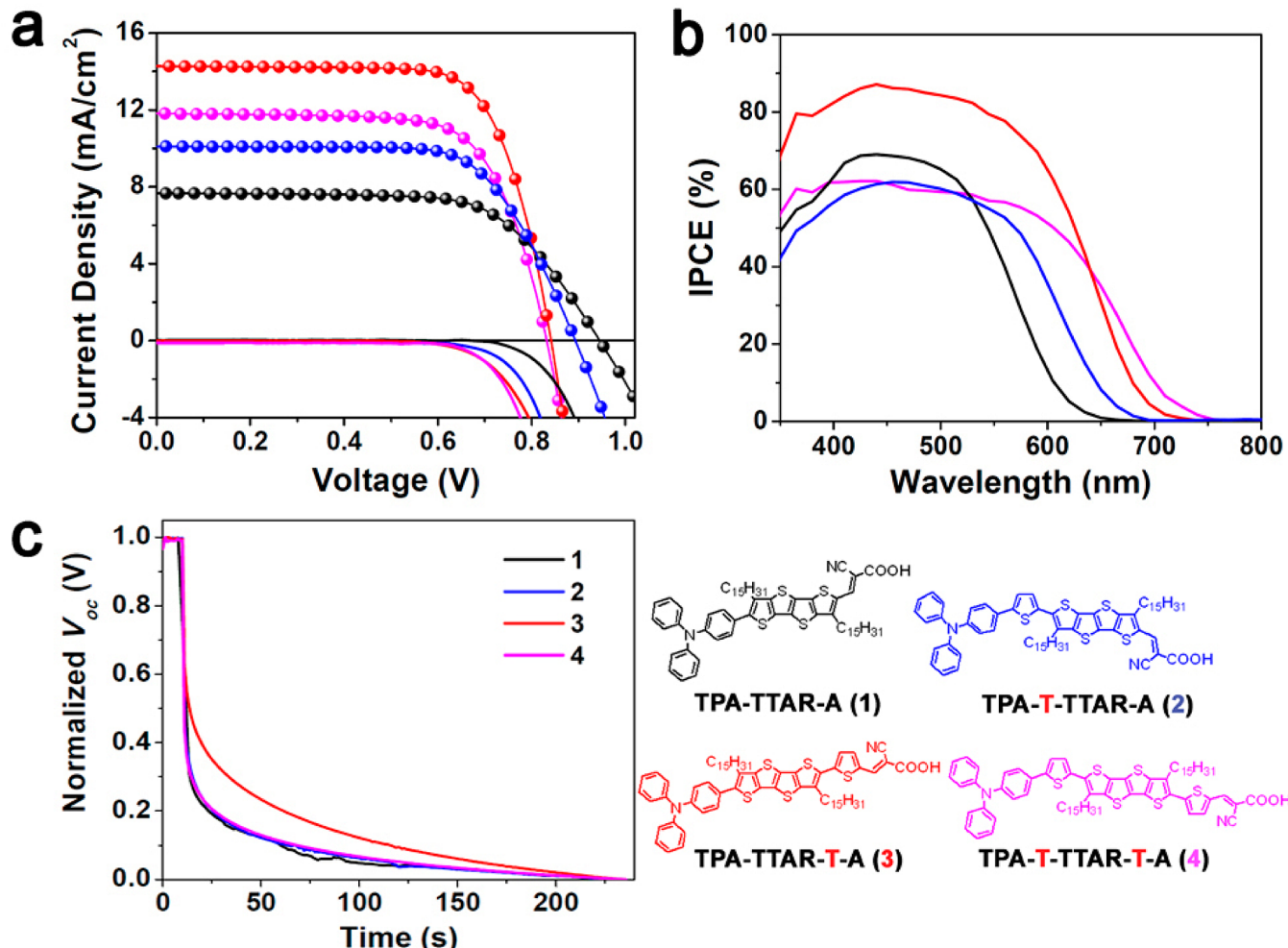


Figure 4. Device characterization for DSSCs based on organic dyes 1–4. (a) Illuminated J – V characteristics; (b) IPCE spectra; (c) Normalized open circuit voltage decay (OCVD).

Dye-Sensitized Solar Cells. DSSCs were fabricated using THF/EtOH (1:1 v/v) solutions of dyes 1–4. The TiO₂ photoelectrode was prepared by electro-spray according to our previous report.⁴⁴ The dye adsorption was performed by immersing the TiO₂ electrode into the dye solution for 10 h at room temperature. After preparation of the Pt counter electrode from H₂PtCl₆ solution, the two electrodes were sealed together using a thermal melt polymer film. The liquid electrolyte was composed of 0.6 M 1-butyl-3-methylimidazolium iodide (BMII), 0.03 M of I₂, 0.1 M of guanidinium thiocyanate (GSCN), and 0.5 M of 4-*tert*-butylpyridine (tBP) in acetonitrile and valeronitrile (85:15 v/v), and was injected between the two electrodes (see more details in Experimental Section). Figure 4a shows representative DSSC device J – V characteristics, while all device parameters are summarized in

Table 2. The DSSC based on the smallest dye 1 shows a modest PCE of 4.76% with a relatively low J_{sc} of 7.66 mA/cm² and a FF of 65.8%. The addition of a thiophene spacer between TPA and TTA (dye 2) substantially increases the PCE to 6.15%, mainly due to the extended absorption enhancing J_{sc} (10.1 mA/cm²). Remarkably, by inserting the thiophene spacer

Table 2. Summary of DSSC Performance Parameters for Dyes 1–4

dye	V_{oc} (V)	J_{sc} (mA/cm ²)	FF (%)	PCE (%)
1	0.946	7.66	65.8	4.76
2	0.893	10.1	68.1	6.15
3	0.833	16.5	73.7	10.1
4	0.832	11.8	70.3	6.91

Table 3. Summary of XRR-Derived SAM Thickness and Molecular Footprint Data for Dyes 1–4 on ALD-Grown TiO₂ Substrates

dye	thickness (Å)	electron density (e/Å ⁻³)	air/dye interface roughness (Å)	TiO ₂ /dye interface roughness (Å)	TiO ₂ layer thickness (Å)	TiO ₂ /SiO ₂ interface roughness (Å)	molecular footprint (Å ²)
1	7.3	0.41	4.5	3.0	16.4	5.0	152
2	6.6	0.41	3.5	2.7	16.5	5.9	183
3	16.8	0.39	5.0	3.5	16.6	3.6	79
4	15.4	0.32	4.7	3.6	16.2	4.3	104

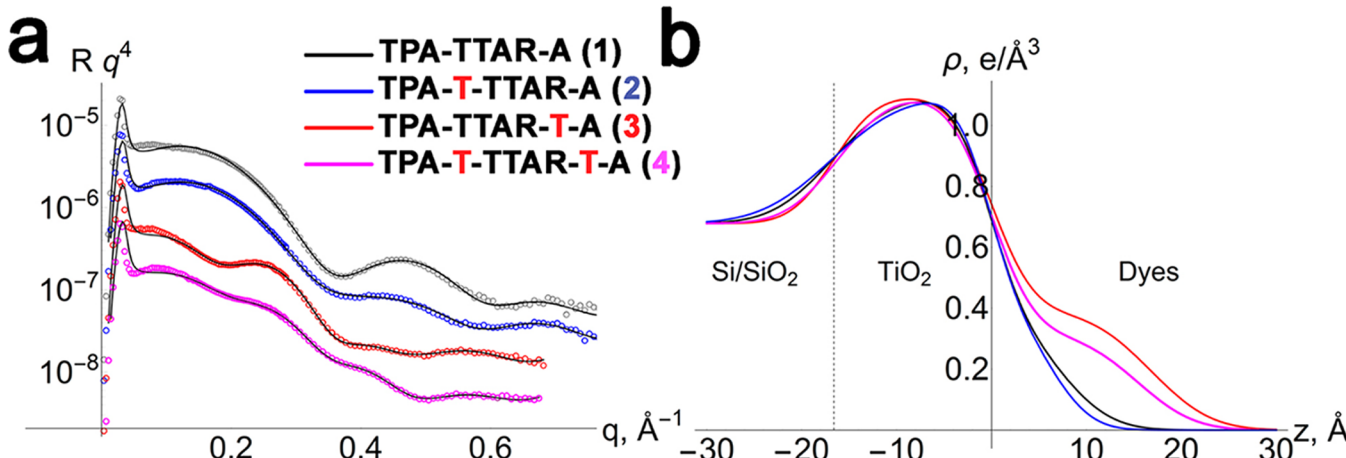


Figure 5. XRR measurements of monolayer dye on TiO₂ surfaces. (a) XRR data and model fits. The top three curves are vertically offset for purposes of clarity. Scattering vector $q = 4\pi \sin(2\theta/2)/\lambda$. (b) Electron density vs depth along the sample surface normal.

between the cyanoacrylic acid and TTA moieties (dye 3), the highest PCE reaches 10.1%, with a $V_{oc} = 0.833$ V, $J_{sc} = 16.5$ mA/cm², and FF = 70.0%. Note that these are the highest DSSC performance metrics for any fused-thiophene based dye sensitizer reported to date, and approach the record PCE of 10.65% for metal-free organic sensitizers recently reported by Yang et al. using a Co(II/III) redox shuttle.²⁰ However, when the thiophene spacers are placed on both donor/acceptor-bridge sides (dye 4), a modest PCE of 6.91% is obtained despite having the lowest HOMO–LUMO energy gap in this series. Interestingly, all four dyes in this study yield very high V_{oc} of 0.832–0.946 V. This experimental data can be explained by the TiO₂ conduction band energy shift as a result of different dye coverages, molecular dipole moments, and/or molecule tilt angles.^{45–49} The dark J – V characteristics also reveal that the dark currents fall in the order of 4 > 3 > 2 > 1, in accord with the trend in the V_{oc} . The spectra of monochromatic incident photon-to-current conversion efficiencies (IPCEs) for the four DSSCs are shown in Figure 4b. These data clearly show that the addition of thiophene units contributes to the extended photon absorption of dyes 2–4 versus the original dye 1, while the highest IPCE for dye 3 is found to exceed 80% from ~385 to ~540 nm.

Open-circuit voltage decay (OCVD) dynamics are presented in Figure 4c to evaluate the lifetimes of photogenerated electrons, τ_n , according to eq 1,^{50,51}

$$\tau_n = -(k_B T/e)(dV_{oc}/dt)^{-1} \quad (1)$$

where k_B is the Boltzmann constant and T is the temperature. Analysis of the OCVD dynamics reveals that of the present four organic DSSCs, the slowest decay dynamics are observed for the dye 3-based cell, followed by dye 2 and dye 4, and the most rapid decay for dye 1, indicating the lowest recombination velocity for the dye 3-based DSSCs.

The charge transport dynamics of the present DSSCs were investigated via electrochemical impedance spectroscopy (EIS) measurements performed under one sun conditions (Figure S2). This analysis is based on the kinetic models of Adachi, Kern, and Bisquert et al.^{52–54} (see detailed analysis in SI). Under open circuit conditions, three semicircles are observed in the frequency range 0.05–150 kHz. Among them, the semicircles in the middle region are attributed to the resistance due to the photoinjection of electrons into the TiO₂ films. It is found that under one sun conditions (with different V_{oc}), dye 3 exhibits the smallest recombination and electron diffusion resistance, suggesting a higher J_{sc} , consistent with the experimental observations. Although this model can compare the cell transport mechanisms at V_{oc} and explains the different cell characteristics (primarily in J_{sc}), it cannot be used to rationalize the voltage dependent recombination rates of the different cells. Nevertheless, these data suggest that chemisorption of dye 3 contributes to the relatively small cell internal resistance, possibly resulting from favorable electron density delocalization and enhanced self-assembly on the TiO₂ surface (see more below). This may reduce the contact area between the TiO₂ and the electrolyte, and in principle, decrease the interception rate of the electrons in the TiO₂ conduction band by I₃⁻.

Chemisorbed Dye Characterization on TiO₂. To obtain further insight into the dye self-organization, molecular orientation, coverage, and aggregation on the TiO₂ surface, XRR measurements were performed on monolayer-coated TiO₂ substrates grown by atomic layer deposition (ALD) onto Si/SiO₂ substrates. The self-assembled monolayer (SAM) chemisorption process was achieved by immersing TiO₂-coated substrates in dye 1–4 solutions in THF/EtOH for ~24 h (see Experimental Section). Similar sample preparation procedures and XRR characterization data were reported by Wagner et al.⁵⁵

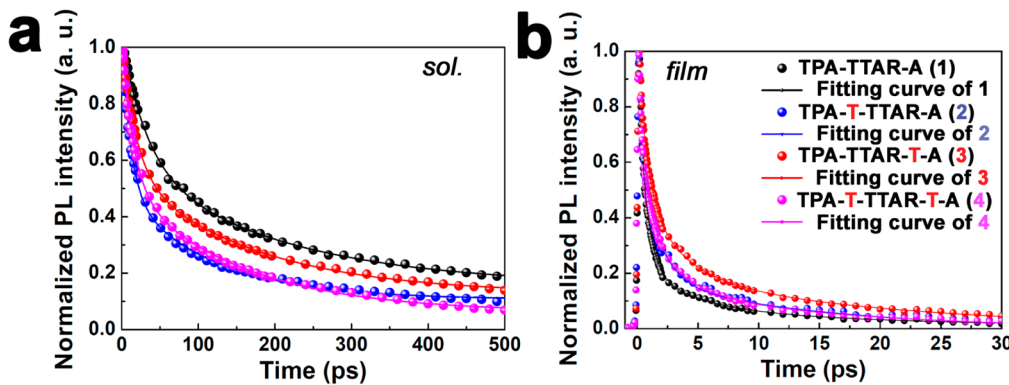


Figure 6. FTR-PL spectra of dyes **1–4**. (a) Dyes **1–4** measured in solution (1:1 v/v in THF + EtOH solvent). (b) Dye-grafted TiO₂ nanoparticle film. The pulse duration, pulse repetition rate, and central wavelength of excitation are 100 fs, 80 MHz, and 420 nm, respectively.

and Griffith et al.⁵⁶ The XRR data were fit according to the procedures reported by Nelson et al.⁵⁷ Interestingly, the XRR data indicate the formation of very thin monolayers (7.3 and 6.6 Å) for the dyes without the thiophene spacer proximate to the cyanoacrylic acid anchoring group (dyes **1** and **2**, respectively). This result suggests that these molecules are not aligned with their long axes perpendicular to the substrate plane (tilt angle = 0°) on the TiO₂ substrates, but rather exhibit significant tilt angles from the surface normal of ~70° (dye **1**) and ~74° (dye **2**), estimated from the DFT-computed molecular lengths of 20.9 Å (dye **1**) and 24.0 Å (dye **2**).⁵⁶ The molecular footprints for these two dye molecules are estimated to be 152 and 183 Å², respectively. Importantly, the addition of a thiophene unit close to the cyanoacrylic acid group in dye **3** greatly enhances film thickness to 16.8 Å, thereby drastically changing the molecular orientation, with a smaller estimated binding tilt angle from the surface normal of only ~48° (estimated molecular length = 24.9 Å), resulting in a significantly smaller molecular footprint of 79 Å². Thus, **3** can form more densely packed monolayers on TiO₂, which not only enhances dye loading for more efficient light harvesting, but also suppresses direct contact between the TiO₂ electrode and the electrolyte, reducing recombination losses. This result is consistent with the highest FF of 70% for DSSCs employing dye **3** (Table 3, Figure 5). On the other hand, despite having the longest backbone (molecular length = 28.9 Å), dye **4** exhibits a slightly reduced monolayer thickness (15.4 Å), thus a larger tilt angle of 58°, and a larger molecular footprint of 104 Å².

To quantify the dye loading in the present DSSCs, the TiO₂ anodes were immersed in 0.30 mM THF/EtOH (1:1) dye solutions, and the dye concentration difference before and after anode soaking was quantified by optical spectrophotometry.⁵⁸ (Figure S3) These experiments indicate that TiO₂ samples coated with dyes **1** and **2** achieve a relatively low dye loading of 2.1×10^{-8} mol/mg and 1.3×10^{-8} mol/mg, respectively, versus those of dyes **3** (7.4×10^{-8} mol/mg) and **4** (6.6×10^{-8} mol/mg). This result is consistent with the smaller molecular footprints and larger tilt angles for these dye molecules as identified in the XRR data. Clearly, introducing a thiophene unit close to the cyanoacrylic anchoring group plays a crucial role in enhancing both vertical dye orientation and dye coverage for dyes **3** and **4** versus **1** and **2**. Additionally, dyes **1** and **3** also show higher dye loadings than dyes **2** and **4**, respectively. This result can be rationalized at the molecular level from the DFT computations which indicate that

thiophene insertion at the donor position undesirably twists molecular backbone (Figure S1), which in other SAM systems is known to suppress molecular self-organization and densification on the substrate surface.^{59–61}

Photophysical Measurements. FTR-PL is a powerful tool for investigating photophysical processes associated with intra- and intermolecular charge transfer and charge injection into TiO₂. Here, the hot and cold electron lifetimes of dyes **1–4** were measured in solution using broadband FTR-PL.^{62,63} The prominent peaks of dyes **1–4** PL spectra are all red-shifted from ~570 nm to ~610 nm over the time range of 2 ps–100 ps (SI, Figure S4). Compared to the time for electron injection from a dye to the TiO₂ nanoparticles (~1 ps),⁶⁴ the time-dependent PL spectrum evolution for the present systems is relatively slow.⁶⁵ The competition between the radiative decay of the excited electron in the dye and the electron injection into TiO₂ nanoparticle mainly occurs at the highest metastable state ($\lambda \sim 570$ nm).⁶⁶ Therefore, hot and cold electron properties must be observed at the emission wavelength of ~570 nm. The electron lifetimes of the present dyes are obtained by fitting the rising (for hot electron) and falling (for cold electron) curves of the TRPL with a two-parameter biexponential decay function (Figures S4 and 6a).⁶⁷ As summarized in Table S1, dye **1**

Table 4. Temporal Characteristics of Photoexcited Electron Dynamics for Dyes **1–4 Adsorbed on TiO₂ Nanoparticles and Their Corresponding DSSC IPCE Metrics**

dye/ TiO ₂	cold electron injection time (exciton dissociation time) (ps)	exciton– exciton annihilation time (ps)	cold electron lifetime (ps)	electron injection efficiency at 420 nm (%)	IPCE at 420 nm (%)
1	0.68	4.35	23.56	97.2	~69
2	1.46	1.47	13.63	90.3	~58
3	0.74	3.08	19.30	96.3	~85
4	0.84	2.77	15.07	94.7	~61

exhibits the longest hot electron lifetime (1.01 ps), matching well with the highest V_{oc} of 0.943 V for the corresponding cells, suggesting efficient hot electron injection into the TiO₂ nanoparticles. In contrast, the hot electron lifetimes of dyes **2–4** are smaller than the instrumental response function (IRF; ~150 fs). Comparing the cold electron decay dynamics, dye **3** exhibits the strongest emission intensity and the longest cold electron lifetime among dyes **2–4** (Figures 6a, at the excitation wavelength of 420 nm) in agreement with its highest IPCE in the series of dyes in this study. Note that the cold electron

lifetime of dye **1** is the longest among the four dyes in this study.

FTR-PL quenching experiments for dye/TiO₂ nanoparticle films were carried out to assess the efficiency of cold electron injection from the dye into the TiO₂ nanoparticles to the DSSC IPCE (Figure 6b). Figure S6 shows the FTR-PL spectra of the dye/TiO₂ nanoparticle films at 0.5 ps, which indicate that the photoexcited electrons in dyes **1–4** relax to the lower metastable state through rapid electron–phonon interactions. In the metastable state, the cold electron injection efficiency can be evaluated at the emission peak wavelength for the dye/TiO₂ nanoparticle films. Figure 6b presents the FTR-PL characteristics of dyes **1–4** adsorbed on the TiO₂ nanoparticle films. To obtain the relaxation times of the cold electrons in dyes **1–4**, the experimental results are fitted according to a triexponential decay function. The three time constants are assigned as the cold electron injection (exciton dissociation) time, the exciton–exciton annihilation time, and the cold electron lifetime. For dyes **1–4**, the trend of cold electron lifetimes in dyes adsorbed on the TiO₂ nanoparticle films is the same as in the solution-based FTR-PL results described above, showing the longest lifetimes for dyes **1** and **3** (23.6 and 19.3 ps, respectively), followed by dyes **4** and **2** (15.1 and 13.6 ps, respectively). Such fast decay dynamics suggest highly efficient electron transfer from the excited states of the dyes to TiO₂. The efficiency of cold electron injection from the dye to TiO₂ nanoparticles can be calculated from the equation $\eta = (1/\tau_{in})/(1/\tau_e + 1/\tau_{in})$,⁶⁸ where τ_{in} is the cold electron injection time and τ_e is the cold electron lifetime. The fitting results of the PL dynamics and the efficiency of cold electron injection are summarized in Table 4. It is evident that the electron injection efficiencies for all four dyes (**1** > **3** > **4** > **2**) are very high (>90% at 420 nm). The relatively high electron injection efficiency for dye **3** agrees very well with its high IPCE of ~85% at 420 nm.

CONCLUSIONS

A novel series of four D–π-bridge–A metal-free organic DSSC dyes based on a highly planar and extensively conjugated TTA bridge were synthesized and characterized. All four dyes exhibit large extinction coefficients for efficient photon absorption. For structural optimization, the role of the thiophene spacer(s) on the molecular donor or acceptor side was the principal focus. Energetically, the addition of a thiophene increases the conjugation length, extends absorption wavelength, and gradually elevates the HOMO energies. The insertion of the thiophene spacer between the TTA bridge unit and the cyanoacrylic acid anchoring sites improves both electron delocalization as well as self-assembly and dye loading on the TiO₂ surface. In contrast, the insertion of the thiophene between the TPA unit and the TTA bridges slightly disrupts molecular backbone planarity, leading to suboptimal dye assembly on TiO₂ and increased recombination losses. Because of its densely packed structure on TiO₂, we demonstrate a highest PCE of 10.1% for dye **3**, one of the highest performing organic dyes reported to date, and the highest for fused-thiophene based sensitizers. We anticipate that further PCE improvements can be obtained by replacing the iodide/triiodide redox couple with a cobalt-based electrolyte. This result suggests that the linear conjugated TTA core is a very promising bridging unit for designing metal-free, organic DSSC dyes. Our investigation also establishes important rules

correlating organic dye molecular design versus self-assembly for further optimizations.

EXPERIMENTAL SECTION

Materials and Synthesis. All chemicals and solvents were of reagent grade and were obtained from Aldrich, Arco, or TCI Chemical Co. Solvents for reactions (toluene, benzene, ether, and THF) were distilled under nitrogen from sodium/benzophenone ketyl, and halogenated solvents were distilled from CaH₂. NMR spectra were measured using a Bruker 300 or 500 MHz spectrometer with chloroform-d and/or tetrahydrofuran-d₈ as solvents. UV–Vis spectra were recorded using a Shimadzu UV3600 UV–vis–NIR spectrophotometer, with EtOH/THF as solvents. Electrospray ionization mass spectrometry was performed using a JMS-700 HRMS spectrometer.

Electrode Preparation and DSSC Assembly. To prepare mesoporous TiO₂ spheres, the aqueous solvent in hydrothermally treated TiO₂ nanoparticle solutions was replaced by ethanol.^{69,70} This solution was then loaded into a syringe equipped with a 27-gauge stainless steel needle. The spaying rate (25 μL/min) for nanoparticle growth was controlled using a syringe pump (KD Scientific model 220). An electric field (12–15 kV) was applied between a metal orifice and the aluminum foil substrate at a distance of 10 cm using a BERTAN Series 230 power supply, and the nanoparticle suspension was electrosprayed onto the aluminum foil. After electrospraying, the as-prepared TiO₂ spheres were made into a paste by stirring with a mixture 0.5 g of the TiO₂ spheres, 100 μL of Triton X-100, 0.2 g of poly(ethylene oxide) (PEO, Adrich, M_w = 100,000) into 3 mL of acetic acid (0.1 M). The resulting TiO₂ paste was then spread onto SnO₂:F coated glass substrates (Pilkington, TEC 8 glass, 8Ω/□, 2.3 mm thick) by doctor-blading to give a flat, smooth surface. Finally, the TiO₂ coated electrode was calcined to remove the polymer under an air flow at 150 °C for 15 min, then at 320 °C for 10 min, and at 500 °C for 30 min, leaving a pure anatase TiO₂ nanosphere film. TiO₂ nanosphere electrode was then immersed in a THF/ethanol solution of the dye molecule (0.30 mM) for 10 h at 25 °C. The dye-adsorbed TiO₂ electrode was then rinsed with ethanol and dried under an N₂ flow. No chenodeoxycholic acid (CDCA) additive was added. The counter-electrode was produced by coating F:SnO₂ glass with a thin layer of a 5 mM solution of H₂PtCl₆ in isopropanol and was then heated at 400 °C for 20 min. The two electrodes were sealed together with thermal melt polymer film (24 μm thick, DuPont). The liquid electrolyte composed of 0.6 M of 1-butyl-3-methylimidazolium iodide (BMII), 0.03 M of iodine, 0.1 M of guanidinium thiocyanate (GSCN) and 0.5 M of 4-*tert*-butylpyridine (tBP) in acetonitrile and valeronitrile (85:15 v/v) was injected between two electrodes.

Solar Cell Measurements. A Newport-Oriel IQE-200 ACDC was used to measure incident photon to charge carrier efficiency (IPCE). The DSSC devices were evaluated under 100 mW/cm² AM1.5G simulated sunlight with a class A solar cell analyzer (Spectra Nova Tech.). A silicon solar cell fitted with a KG3 filter tested and certified by the National Renewable Energy Laboratory (NREL) was used for calibration. The KG3 filter accounts for the different light absorption between the dye-sensitized solar cell and the silicon solar cell, and it ensures that the spectral mismatch correction factor approaches unity.

Electrochemical Measurements. Electrochemistry was performed on a C3 Cell Stand electrochemical station equipped with BAS Epsilon software (Bioanalytical Systems, Inc., Lafayette, IN), a glassy carbon working electrode, a Pt-wire counter electrode and a Ag-wire reference electrode. Dyes **1–4** were dissolved in anhydrous dichloromethane (~1 mg/mL) along with Bu₄N(PF₆) (0.1 M) electrolyte. All scans were performed at 100 mV/s scan rate under Nitrogen atmosphere. A ferrocene/ferrocenium redox couple was used as an internal standard.

XRR Measurements. XRR curves were obtained on Rigaku Smartlab with standard slits for a 300 mm goniometer. Curves of Rq4 vs q were fitted by Motofit with error bars which included counting and machine measurement errors, and edge effects for small q regions. TiO₂ films of ~16–17 Å were prepared via atomic layer deposition (ALD) on bare Si substrates, and subsequently sintered at 500 °C for 2

to obtain the TiO₂ anatase phase. XRR measurements of these TiO₂ films on Si shows crystalline randomly oriented TiO₂ in the anatase phase. XRR samples were prepared by immersing the TiO₂ coated substrates in THF/EtOH solvent (1:1) for dye 1–4, and allowing self-assembly monolayer (SAM) growth over 24 h. The substrates were subsequently washed with pure solvents.

EIS Measurements and Analysis. The electrochemical impedance results were measured under the same light illumination with a Solartron 1260 impedance analyzer and a Solartron 1287 potentiostat with the device at V_{oc} .

Femtosecond Time-Resolved Photoluminescence (FTR-PL). To understand the photoexcited electron dynamics in dyes 1–4, the FTR-PL was measured by the sum-frequency technique (FluoMax, IB Photonics Ltd.). The dyes dissolved in THF/EtOH solutions were pumped at the wavelength of 420 nm. To observe the ultrashort lifetime of hot electrons, the pumping laser was focused onto the sample with a short Rayleigh length which gives an instrument response function of ~150 fs.

ASSOCIATED CONTENT

Supporting Information

Synthetic procedures and characterization data of all new compounds. Details for all device characterizations. This material is available free of charge via the Internet at <http://pubs.acs.org>.

AUTHOR INFORMATION

Corresponding Authors

*bedzyk@northwestern.edu

*ratner@northwestern.edu

*r-chang@northwestern.edu

*a-facchetti@northwestern.edu

*mcchen@ncu.edu.tw

*t-marks@northwestern.edu

Author Contributions

#N.Z., K.P., and B.L. contributed equally.

Notes

The authors declare no competing financial interest.

ACKNOWLEDGMENTS

This research is supported as part of the ANSER Center, an Energy Frontier Research Center funded by the U.S. Department of Energy, Office of Science, and Office of Basic Energy Sciences under Award Number DE-SC0001059. We thank the NSF-MRSEC program through the Northwestern University Materials Research Science and Engineering Center for characterization facilities (DMR-1121262) and Institute for Sustainability and Energy at Northwestern (ISEN) for partial equipment funding. Financial assistance for this research was also provided by the National Science Council, Taiwan, Republic of China (Grant Numbers NSC102-2113-M-008-004 and NSC102-2923-M-008-004-MY2).

REFERENCES

- Oregan, B.; Grätzel, M. *Nature* **1991**, *353*, 737.
- Mathew, S.; Yella, A.; Gao, P.; Humphry-Baker, R.; CurchodBasile, F. E.; Ashari-Astani, N.; Tavernelli, I.; Rothlisberger, U.; Nazeeruddin, M. K.; Grätzel, M. *Nat. Chem.* **2014**, *6*, 242.
- Bach, U.; Lupo, D.; Comte, P.; Moser, J. E.; Weissertel, F.; Salbeck, J.; Spreitzer, H.; Grätzel, M. *Nature* **1998**, *395*, 583.
- Grätzel, M. *Inorg. Chem.* **2005**, *44*, 6841.
- Hagfeldt, A.; Grätzel, M. *Acc. Chem. Res.* **2000**, *33*, 269.
- Yella, A.; Mai, C.-L.; Zakeeruddin, S. M.; Chang, S.-N.; Hsieh, C.-H.; Yeh, C.-Y.; Grätzel, M. *Angew. Chem.* **2014**, *53*, 2973.

- Yella, A.; Lee, H.-W.; Tsao, H. N.; Yi, C.; Chandiran, A. K.; Nazeeruddin, M. K.; Diau, E. W.-G.; Yeh, C.-Y.; Zakeeruddin, S. M.; Grätzel, M. *Science* **2011**, *334*, 629.
- Hagfeldt, A.; Boschloo, G.; Sun, L. C.; Kloo, L.; Pettersson, H. *Chem. Rev.* **2010**, *110*, 6595.
- Jiao, Y.; Zhang, F.; Grätzel, M.; Meng, S. *Adv. Funct. Mater.* **2013**, *23*, 424.
- Kozma, E.; Concina, I.; Braga, A.; Borgese, L.; Depero, L. E.; Vomiero, A.; Sberveglieri, G.; Catellani, M. *J. Mater. Chem.* **2011**, *21*, 13785.
- Qu, S. Y.; Wu, W. J.; Hua, J. L.; Kong, C.; Long, Y. T.; Tian, H. *J. Phys. Chem. C* **2010**, *114*, 1343.
- Kim, D.; Ghicov, A.; Albu, S. P.; Schmuki, P. *J. Am. Chem. Soc.* **2008**, *130*, 16454.
- Sauvage, F.; Di Fonzo, F.; Bassi, A. L.; Casari, C. S.; Russo, V.; Divitini, G.; Ducati, C.; Bottani, C. E.; Comte, P.; Graetzel, M. *Nano Lett.* **2010**, *10*, 2562.
- He, J. X.; Wu, W. J.; Hua, J. L.; Jiang, Y. H.; Qu, S. Y.; Li, J.; Long, Y. T.; Tian, H. *J. Mater. Chem.* **2011**, *21*, 6054.
- Kakiage, K.; Aoyama, Y.; Yano, T.; Otsuka, T.; Kyomen, T.; Unno, M.; Hanaya, M. *Chem. Commun.* **2014**, *50*, 6379.
- Cao, Y.; Cai, N.; Wang, Y.; Li, R.; Yuan, Y.; Wang, P. *Phys. Chem. Chem. Phys.* **2012**, *14*, 8282.
- Yum, J.-H.; Holcombe, T. W.; Kim, Y.; Rakstys, K.; Moehl, T.; Teuscher, J.; Delcamp, J. H.; Nazeeruddin, M. K.; Grätzel, M. *Sci. Rep.* **2013**, *3*, 2446.
- Yum, J.-H.; Baranoff, E.; Kessler, F.; Moehl, T.; Ahmad, S.; Bessho, T.; Marchioro, A.; Ghadiri, E.; Moser, J.-E.; Yi, C.; Nazeeruddin, M. K.; Grätzel, M. *Nat. Commun.* **2012**, *3*, 631.
- Zhang, M.; Wang, Y.; Xu, M.; Ma, W.; Li, R.; Wang, P. *Energy Environ. Sci.* **2013**, *6*, 2944.
- Yang, J.; Ganeshan, P.; Teuscher, J.; Moehl, T.; Kim, Y. J.; Yi, C.; Comte, P.; Pei, K.; Holcombe, T. W.; Nazeeruddin, M. K.; Hua, J.; Zakeeruddin, S. M.; Tian, H.; Grätzel, M. *J. Am. Chem. Soc.* **2014**, *136*, 5722.
- Mishra, A.; Fischer, M. K. R.; Bauerle, P. *Angew. Chem.* **2009**, *48*, 2474.
- Wang, Z. S.; Koumura, N.; Cui, Y.; Takahashi, M.; Sekiguchi, H.; Mori, A.; Kubo, T.; Furube, A.; Hara, K. *Chem. Mater.* **2008**, *20*, 3993.
- Wang, Z. S.; Cui, Y.; Dan-Oh, Y.; Kasada, C.; Shinpo, A.; Hara, K. *J. Phys. Chem. C* **2007**, *111*, 7224.
- Chen, H. J.; Huang, H.; Huang, X. W.; Cliford, J. N.; Forneli, A.; Palomares, E.; Zheng, X. Y.; Zheng, L. P.; Wang, X. Y.; Shen, P.; Zhao, B.; Tan, S. T. *J. Phys. Chem. C* **2010**, *114*, 3280.
- Choi, H.; Raabe, I.; Kim, D.; Teocoli, F.; Kim, C.; Song, K.; Yum, J. H.; Ko, J.; Nazeeruddin, M. K.; Grätzel, M. *Chem.—Eur. J.* **2010**, *16*, 1193.
- Hagberg, D. P.; Marinado, T.; Karlsson, K. M.; Nonomura, K.; Qin, P.; Boschloo, G.; Brinck, T.; Hagfeldt, A.; Sun, L. *J. Org. Chem.* **2007**, *72*, 9550.
- Haid, S.; Marszalek, M.; Mishra, A.; Wielopolski, M.; Teuscher, J.; Moser, J. E.; Humphry-Baker, R.; Zakeeruddin, S. M.; Grätzel, M.; Bauerle, P. *Adv. Funct. Mater.* **2012**, *22*, 1291.
- Cai, N.; Moon, S.-J.; Cevey-Ha, L.; Moehl, T.; Humphry-Baker, R.; Wang, P.; Zakeeruddin, S. M.; Grätzel, M. *Nano Lett.* **2011**, *11*, 1452.
- Joly, D.; Pellejà, L.; Narbey, S.; Oswald, F.; Chiron, J.; Clifford, J. N.; Palomares, E.; Demadrille, R. *Sci. Rep.* **2014**, *4*, 4033.
- Kim, B.-G.; Chung, K.; Kim, J. *Chem.—Eur. J.* **2013**, *19*, 5220.
- Teng, C.; Yang, X. C.; Yang, C.; Li, S. F.; Cheng, M.; Hagfeldt, A.; Sun, L. C. *J. Phys. Chem. C* **2010**, *114*, 9101.
- Wang, M. K.; Xu, M. F.; Shi, D.; Li, R. Z.; Gao, F. F.; Zhang, G. L.; Yi, Z. H.; Humphry-Baker, R.; Wang, P.; Zakeeruddin, S. M.; Grätzel, M. *Adv. Mater.* **2008**, *20*, 4460.
- Kwon, T. H.; Armel, V.; Nattestad, A.; MacFarlane, D. R.; Bach, U.; Lind, S. J.; Gordon, K. C.; Tang, W. H.; Jones, D. J.; Holmes, A. B. *J. Org. Chem.* **2011**, *76*, 4088.

- (34) Qin, H.; Wenger, S.; Xu, M.; Gao, F.; Jing, X.; Wang, P.; Zakeeruddin, S. M.; Gratzel, M. *J. Am. Chem. Soc.* **2008**, *130*, 9202.
- (35) Zhang, G. L.; Bala, H.; Cheng, Y. M.; Shi, D.; Lv, X. J.; Yu, Q. J.; Wang, P. *Chem. Commun.* **2009**, 2198.
- (36) Fong, H. H.; Pozdin, V. A.; Amassian, A.; Malliaras, G. G.; Smilgies, D. M.; He, M. Q.; Gasper, S.; Zhang, F.; Sorensen, M. *J. Am. Chem. Soc.* **2008**, *130*, 13202.
- (37) Youn, J.; Huang, P.-Y.; Huang, Y.-W.; Chen, M.-C.; Lin, Y.-J.; Huang, H.; Ortiz, R. P.; Stern, C.; Chung, M.-C.; Feng, C.-Y.; Chen, L.-H.; Facchetti, A.; Marks, T. *J. Adv. Funct. Mater.* **2012**, *22*, 48.
- (38) Kim, C.; Chen, M.-C.; Chiang, Y.-J.; Guo, Y.-J.; Youn, J.; Huang, H.; Liang, Y.-J.; Lin, Y.-J.; Huang, Y.-W.; Hu, T.-S.; Lee, G.-H.; Facchetti, A.; Marks, T. *J. Org. Electron.* **2010**, *11*, 801.
- (39) Kumaresan, P.; Vegiraju, S.; Ezhumalai, Y.; Yau, S.; Kim, C.; Lee, W.-H.; Chen, M.-C. *Polymers* **2014**, *6*, 2645.
- (40) Nazeeruddin, M. K.; Kay, A.; Rodicio, I.; Humphrybaker, R.; Muller, E.; Liska, P.; Vlachopoulos, N.; Gratzel, M. *J. Am. Chem. Soc.* **1993**, *115*, 6382.
- (41) Chen, H.; Huang, H.; Huang, X.; Clifford, J. N.; Forneli, A.; Palomares, E.; Zheng, X.; Zheng, L.; Wang, X.; Shen, P.; Zhao, B.; Tan, S. *J. Phys. Chem. C* **2010**, *114*, 3280.
- (42) Youn, J.; Kewalramani, S.; Emery, J. D.; Shi, Y.; Zhang, S.; Chang, H.-C.; Liang, Y.-j.; Yeh, C.-M.; Feng, C.-Y.; Huang, H.; Stern, C.; Chen, L.-H.; Ho, J.-C.; Chen, M.-C.; Bedzyk, M. J.; Facchetti, A.; Marks, T. *J. Adv. Funct. Mater.* **2013**, *23*, 3850.
- (43) Numata, Y.; Ashraful, I.; Shirai, Y.; Han, L. Y. *Chem. Commun.* **2011**, *47*, 6159.
- (44) Lee, B.; Stoumpos, C. C.; Zhou, N.; Hao, F.; Malliakas, C.; Yeh, C.-Y.; Marks, T. J.; Kanatzidis, M. G.; Chang, R. P. H. *J. Am. Chem. Soc.* **2014**, *136*, 15379.
- (45) De Angelis, F.; Fantacci, S.; Selloni, A.; Grätzel, M.; Nazeeruddin, M. K. *Nano Lett.* **2007**, *7*, 3189.
- (46) Chen, P.; Yum, J. H.; Angelis, F. D.; Mosconi, E.; Fantacci, S.; Moon, S.-J.; Baker, R. H.; Ko, J.; Nazeeruddin, M. K.; Grätzel, M. *Nano Lett.* **2009**, *9*, 2487.
- (47) Kusama, H.; Orita, H.; Sugihara, H. *Langmuir* **2008**, *24*, 4411.
- (48) Ronca, E.; Pastore, M.; Belpassi, L.; Tarantelli, F.; De Angelis, F. *Energy Environ. Sci.* **2013**, *6*, 183.
- (49) Feng, J.; Jiao, Y.; Ma, W.; Nazeeruddin, M. K.; Grätzel, M.; Meng, S. *J. Phys. Chem. C* **2013**, *117*, 3772.
- (50) Bisquert, J.; Zaban, A.; Greenshtein, M.; Mora-Seró, I. *J. Am. Chem. Soc.* **2004**, *126*, 13550.
- (51) Zaban, A.; Greenshtein, M.; Bisquert, J. *ChemPhysChem* **2003**, *4*, 859.
- (52) Adachi, M.; Sakamoto, M.; Jiu, J. T.; Ogata, Y.; Isoda, S. *J. Phys. Chem. B* **2006**, *110*, 13872.
- (53) Bisquert, J. *J. Phys. Chem. B* **2002**, *106*, 325.
- (54) Kern, R.; Sastrawan, R.; Ferber, J.; Stangl, R.; Luther, J. *Electrochim. Acta* **2002**, *47*, 4213.
- (55) Wagner, K.; Griffith, M. J.; James, M.; Mozer, A. J.; Wagner, P.; Triani, G.; Officer, D. L.; Wallace, G. G. *J. Phys. Chem. C* **2011**, *115*, 317.
- (56) Griffith, M. J.; James, M.; Triani, G.; Wagner, P.; Wallace, G. G.; Officer, D. L. *Langmuir* **2011**, *27*, 12944.
- (57) Nelson, A. *J. Appl. Crystallogr.* **2006**, *39*, 273.
- (58) Watson, T.; Holliman, P.; Worsley, D. *J. Mater. Chem.* **2011**, *21*, 4321.
- (59) Song, C. K.; Luck, K. A.; Zhou, N.; Zeng, L.; Heitzer, H. M.; Manley, E. F.; Goldman, S.; Chen, L. X.; Ratner, M. A.; Bedzyk, M. J.; Chang, R. P. H.; Hersam, M. C.; Marks, T. J. *J. Am. Chem. Soc.* **2014**, *136*, 17762.
- (60) Chesneau, F.; Schupbach, B.; Szelagowska-Kunstman, K.; Ballav, N.; Cyganik, P.; Terfort, A.; Zharnikov, M. *Phys. Chem. Chem. Phys.* **2010**, *12*, 12123.
- (61) Voznyy, O.; Dubowski, J. *J. Langmuir* **2008**, *24*, 13299.
- (62) Fakis, M.; Anestopoulos, D.; Giannetas, V.; Persephonis, P.; Mikroyannidis, J. *J. Phys. Chem. B* **2006**, *110*, 12926.
- (63) Fakis, M.; Giannetas, V.; Mikroyannidis, J. *Dyes Pigm.* **2010**, *87*, 44.
- (64) Hilgendorff, M.; Sundstrom, V. *J. Phys. Chem. B* **1998**, *102*, 10505.
- (65) Hara, K.; Wang, Z. S.; Sato, T.; Furube, A.; Katoh, R.; Sugihara, H.; Dan-Oh, Y.; Kasada, C.; Shinpo, A.; Suga, S. *J. Phys. Chem. B* **2005**, *109*, 15476.
- (66) Cherepy, N. J.; Smestad, G. P.; Grätzel, M.; Zhang, J. Z. *J. Phys. Chem. B* **1997**, *101*, 9342.
- (67) Chang, S. H.; Chiang, C.-H.; Cheng, H.-M.; Tai, C.-Y.; Wu, C.-G. *Opt. Lett.* **2013**, *38*, 5342.
- (68) Deibel, C.; Strobel, T.; Dyakonov, V. *Phys. Rev. Lett.* **2009**, *103*, 036402.
- (69) Lee, B.; Buchholz, D. B.; Guo, P. J.; Hwang, D. K.; Chang, R. P. H. *J. Phys. Chem. C* **2011**, *115*, 9787.
- (70) Lee, B.; Hwang, D. K.; Guo, P. J.; Ho, S. T.; Buchholtz, D. B.; Wang, C. Y.; Chang, R. P. H. *J. Phys. Chem. B* **2010**, *114*, 14582.